ELSEVIER

Journal of Volcanology and Geothermal Research 115 (2002) 233–255

Journal of volcanology and geothermal research

www.elsevier.com/locate/jvolgeores

Surface effects of faulting and deformation resulting from magma accumulation at the Hengill triple junction, SW Iceland, 1994–1998

Amy E. Clifton [a,*], Freysteinn Sigmundsson [a], Kurt L. Feigl [b], Gunnar Guðmundsson [c], Thóra Árnadóttir [a]

[a] *Nordic Volcanological Institute, Grensásvegur 50, 108 Reykjavík, Iceland*
[b] *CNRS UMR 5562, Observatoire Midi Pyrénées, 14 Avenue E. Belin, 31400 Toulouse, France*
[c] *Icelandic Meteorological Office, Bustadavegur 9, 103 Reykjavík, Iceland*

Received 28 March 2001; accepted 30 September 2001

Abstract

The Hengill triple junction, SW Iceland, is subjected to both tectonic extension and shear, causing seismicity related to strike-slip and normal faulting. Between 1994 and 1998, the area experienced episodic swarms of enhanced seismicity culminating in a $M_L = 5.1$ earthquake on June 4, 1998 and a $M_L = 5$ earthquake on November 13, 1998. Geodetic measurements, using Global Positioning System (GPS), leveling and Synthetic Aperture Radar Interferometry (InSAR) detected maximum uplift of 2 cm/yr and expansion between the Hrómundartindur and Grensdalur volcanic systems. A number of faults in the area generated meter-scale surface breaks. Geographic Information System (GIS) software has been used to integrate structural, field and geophysical data to determine how the crust failed, and to evaluate how much of the recent activity focused on zones of pre-existing weaknesses in the crust. Field data show that most surface effects can be attributed to the June 4, 1998 earthquake and have occurred along or adjacent to old faults. Surface effects consist of open gashes in soil, shattering of lava flows, rockfall along scarps and within old fractures, loosened push-up structures and landslides. Seismicity in 1994–1998 was distributed asymmetrically about the center of uplift, with larger events migrating toward the main fault of the June 4, 1998 earthquake. Surface effects are most extensive in the area of greatest structural complexity, where N- and E-trending structures related to the transform boundary intersect NE-trending structures related to the rift zone. InSAR, GPS, and field observations have been used in an attempt to constrain slip along the trace of the fault that failed on June 4, 1998. Geophysical and field data are consistent with an interpretation of distributed slip along a segmented right-lateral strike-slip fault, with slip decreasing southward along the fault plane. We suggest a right step or right bend between fault segments to explain local deformation near the fault.

Keywords: volcano deformation; faulting; Iceland; Hengill triple junction

1. Introduction

The Hengill, Hrómundartindur and Grensdalur volcanic systems are located at the Hengill triple

* Corresponding author. Fax: +354-562-9767.
E-mail address: amy@norvol.hi.is (A.E. Clifton).

0377-0273/02/$ – see front matter
PII: S0377-0273(01)00319-5

junction at which the oblique Reykjanes Peninsula (rift) zone (RP), the Western Volcanic (rift) zone (WVZ) and the South Iceland Seismic (transform) zone (SISZ) meet in SW Iceland (Sæmundsson, 1992; Fig. 1). Two large high-temperature geothermal fields, Nesjavellir and Ölkelduháls, are associated with the Hengill and Hrómundartindur volcanoes, respectively, and a smaller geothermal field in Hveragerði is associated with the easternmost and oldest Grensdalur system (Sæmundsson, 1992). Nine $M \geq 5$ earthquakes are known to have occurred in the area between 1546 and 1955. In 1955, a $M = 5.5$ event damaged homes and greenhouses in Hveragerði and caused rockfall in valleys to the north (Halldórsson and Stefánsson, 1986,1987).

The Hengill triple junction exhibited a high rate of background seismicity after a permanent Icelandic regional seismograph network was established in 1974 (Foulger, 1988a). About 50% of the earthquakes had focal mechanisms consistent with either normal or strike-slip faulting related to plate motion. The other half of the earthquakes were concentrated in the geothermal areas and exhibited non-double-couple mechanisms characteristic of extensional failure due to circulating fluids (Foulger, 1988b).

A period of markedly enhanced seismicity began in the area in July 1994 and continued through 1998, with more than 80 000 small earthquakes occurring. Seismicity increased in 1995, decreased in 1996 and then increased significantly in 1997 and 1998. Activity culminated on June 4, 1998 when a $M_L = 5.1$ event occurred along a previously unmapped fault 3.7 km due west of the uplift center (see Fig. 1). Aftershocks concentrated along a N–S trend extending approximately 10 km to the south, and GPS data indicated that approximately 30 cm of right-lateral strike-slip occurred along a N-trending, sub-vertical fault plane (Árnadóttir et al., 1999). On November 13, 1998, another large earthquake occurred 12 km south of the June event. This $M_L = 5.0$ event triggered a swarm of earthquakes, including 10 events with $M_L \geq 3.0$, along an E–W-trending zone approximately 10–15 km long and 2 km wide (Rögnvaldsson et al., 1998). GPS measurements (Hreinsdóttir et al., 2001) indicate that left-lateral shear occurred across that fault zone. Focal mechanisms and relative locations for the largest of these events are consistent with right-lateral strike-slip on many small N–S-trending planes (Rögnvaldsson et al., 1998) that may have failed in a 'bookshelf-faulting' style of deformation (e.g. Sigmundsson et al., 1995). However, based on these data alone, motion along an underlying E–W-trending fault cannot be discounted.

The 1994–1998 seismic period was associated with widespread crustal uplift. Sparse leveling data covering the period from 1986 to 1995 and GPS data from 1991 to 1994 show surface deformation consistent with a Mogi point source of pressure at about 6.5 km depth, interpreted to reflect magma accumulation centered under the Hrómundartindur volcanic system (Sigmundsson et al., 1997). Further GPS and leveling surveys conducted by the National Energy Authority also detected uplift in the area (Thorbergsson and Vigfusson, 1998). GPS data from Hreinsdóttir et al. (2001) covering the period from 1995 to 1998 suggest that there may have been a very steep uplift gradient in the area between the Grensdalur and Hrómundartindur volcanoes. After the June 4, 1998 earthquake, uplift slowed down somewhat between the June 4 and the November 13, 1998 earthquakes, and became insignificant between November, 1998 and March, 1999 (Thorbergsson, 1999; Hreinsdóttir et al.,

Fig. 1. (A) Tectonic map of Iceland (after Einarsson and Sæmundsson, 1992) showing volcanic systems and plate boundary segments. Arrows show direction and rate of absolute plate motion (DeMets et al., 1994). Box encloses area shown in (B). Black oval within box shows location of Hengill triple junction. (B) Topographic grid of Reykjanes Peninsula. White box encloses study area shown in (C). (C) Aerial photomosaic of study area in the Hengill triple junction. Black lines show the three volcanic systems (Sæmundsson, 1992) located at the Hengill triple junction. White circle with cross represents 1 km radius around center of volcanic uplift as determined from interferometry (Feigl et al., 2000). White filled star shows epicenter of June 4, 1998 $M = 5.1$ earthquake. White unfilled star shows epicenter of November 13, 1998 $M = 5.0$ earthquake. Locations identified are mentioned frequently in the text.

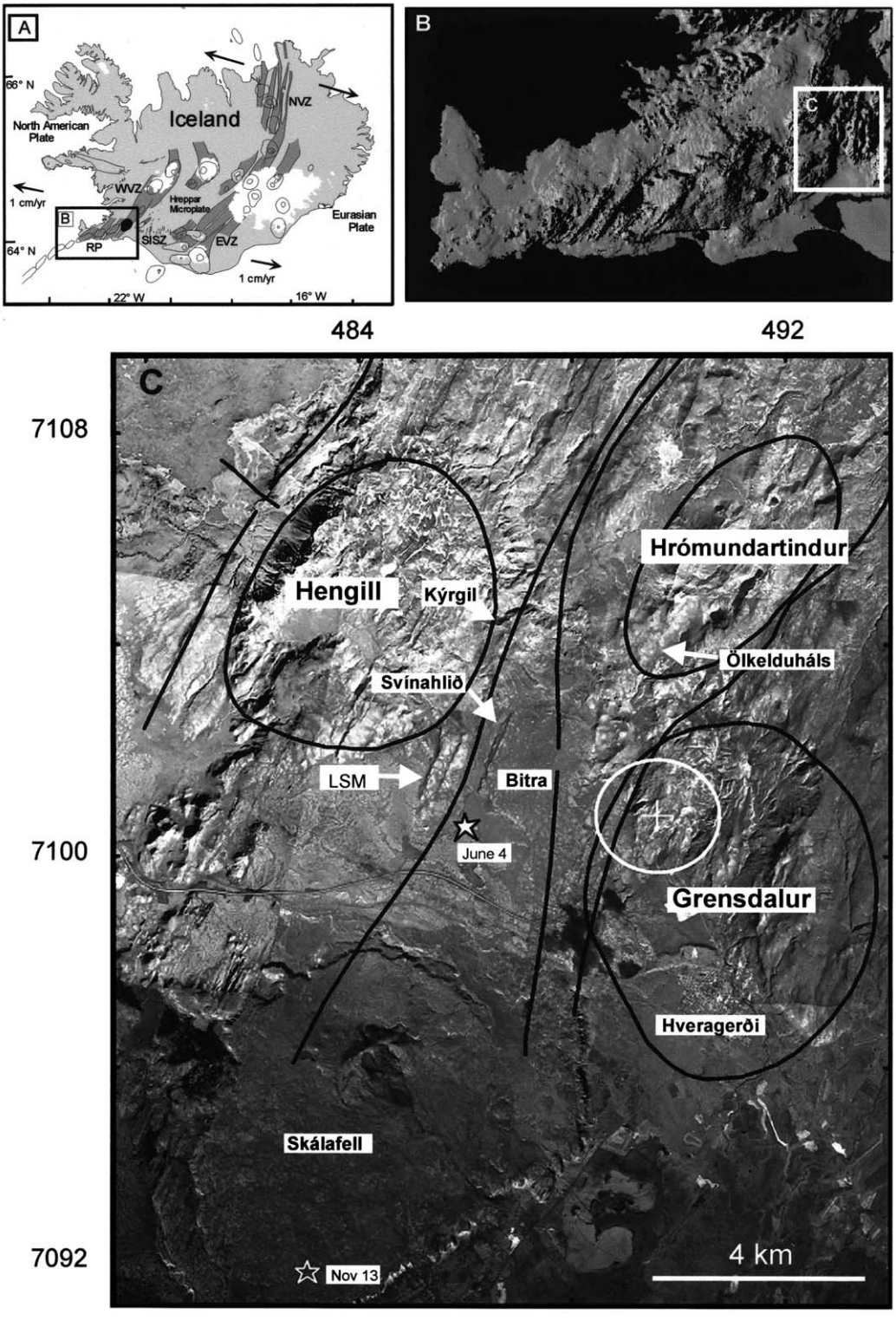
A
66° N
Iceland
NVZ
North American Plate
WVZ
1 cm/yr
Hreppar Microplate
Eurasian Plate
B
SISZ
EVZ
RP
64° N
1 cm/yr
22° W
16° W
B
C
484
492
C
7108
Hengill
Kýrgil
Hrómundartindur
Ölkelduháls
Svínahlið
LSM
Bitra
7100
June 4
Grensdalur
Hveragerði
Skálafell
7092
Nov 13
4 km

2001). A continuous GPS network established in the area between March and May, 1999 has detected no significant uplift (0 ± 5 mm/yr), and only 2 mm eastward motion in the 12 months since measurements began (Árnadóttir et al., 2000).

Feigl et al. (2000) examined a series of interferograms covering the period from 1993 to 1998 and noted that the principal deformation signal was a concentric pattern of fringes. This was interpreted as a relatively constant 19 ± 2 mm/yr rate of uplift around a point source of magma accumulation located at UTM coordinates Easting 48953, Northing 7100772, on the northwestern edge of the Grensdalur volcanic system, at about 7 km depth (see circle on all figures). This revised estimate of the uplift center is within the uncertainties of the center estimated by Sigmundsson et al. (1997). The InSAR results show that the location of the uplift center had been stable for the 5-yr period.

In this paper, we address several unresolved questions. These include the following: (1) How are the observed surface effects related to the uplift and/or earthquakes? (2) How much disruption occurred along old versus new faults? (3) Did fault movement or shaking cause the observed surface effects? (4) Why were earthquakes distributed asymmetrically with respect to the uplift center? To answer these questions, we use GIS to synthesize datasets including a detailed map of the surface effects, earthquake locations, topographic lineaments, previously mapped faults and geothermal springs (Sæmundsson, 1995), and InSAR interferograms.

2. Methods

Our multidisciplinary approach requires integrating various data types and creating a base map on which to display data spatially. We compiled a mosaic of orthorectified, georeferenced aerial photographs of the study area and plotted data directly onto the photographs. Displaying geophysical data such as earthquake locations and geodetic measurements on aerial photographs allowed us to see their relationship to local structures and geology more clearly than is possible on a topographic base map. The photographs also enabled us to more precisely identify areas that bore further investigation and to find them quickly in the field by using pre-set GPS points. Between August, 1999 and October, 2000 we conducted fieldwork systematically within a 1-km radius of the center of uplift and in the areas of greatest seismicity. Special attention was paid to the area along the trend of aftershocks from the June 4, 1998 event and along the trend of the large earthquake swarm of November 13, 1998.

2.1. Orthorectification of aerial photographs

Scanned aerial photographs of photogrammetric quality at a scale of 1:25 000 were obtained from the National Land Survey of Iceland. These were imported into ERDAS Imagine software for processing. A digital elevation model (DEM) was created from a 1:50 000 digitized map with a contour interval of 20 m using ArcInfo. The DEM was then imported into ERDAS Imagine for use in the orthorectification process. Once orthorectified, nine photographs were made into a photomosaic. In spite of endless efforts to minimize errors in rectifying the images, variable distortion typically on the order of meters remains on the outer edges of most photographs. This is primarily because man-made features are absent in the area, and natural features whose geometry may change with time (e.g. lake shorelines and bends in streams) were, by necessity, used as ground control points in the rectification process. In addition, the photos used to make the mosaic were taken at different times of the year, and in different years (1989 and 1991) so that the lighting varies more than is optimal for accurately identifying specific points on the ground. All data were projected into the UTM coordinate system, zone 27 N, International 1909 spheroid, Hjorsey datum.

2.2. Fieldwork

Field data consist of measurements of rupture traces and point locations of rockfall and other local surface effects (see 3.1. Type A: fresh fractures in soil cover). The term 'surface effects' is

used here to denote the visible effects of crustal deformation at the free surface of the earth. These include opening mode fractures in rock and/or soil, sinkholes, and downslope movement of material (e.g. rockfall, slump). We make a distinction between these easily visible geologic features and smaller or deeper crustal deformation which may require geophysical instrumentation to be detected.

Locations of these features were mapped as either points, lines or areas using the Trimble differential GPS Pathfinder Pro XR GIS data collection system. The stated horizontal accuracy of the unit is 50 cm ± 1 ppm on a second-by-second basis and vertical accuracy of submeter ± 2 ppm on a second-by-second basis. The Trimble TSC1 data logger was used to store data. Trimble Pathfinder software was used for processing and exporting the data as shapefiles into the Imagine program.

2.3. Earthquake data

Earthquake data used here come from the SIL (South Iceland Lowland) earthquake database, maintained by the Icelandic Meteorological Office (Stefánsson et al., 1993). Data were imported into ArcInfo and turned into point coverages to be used in the GIS database. In an effort to minimize location error, some events were eliminated according to the following parameters: depth < 1.0 km; depth error 0.0 (i.e. depth fixed); gap $> 180°$, where gap is the maximum angular separation between stations; rms error for weighted travel time residuals > 0.2 s; number of S-wave arrivals < 3; number of P-wave arrivals < 2. Table 1 shows the precision in horizontal location of the data we retained. Vertical precision is smaller (< 1 km) than horizontal precision. Installation of two new stations in the network in late 1996 increased location precision significantly. Location precision (± 500 m) for the majority of $M \geq 3$ events was better than that for smaller events both before and after the installation of the new stations.

2.4. InSAR

We use interferograms of the Hengill area covering the years 1993–1998 calculated from ERS data by Gasperi (1999) and Bretar (2000). Feigl et al. (2000) analyzed these interferograms to determine the volcanic uplift signal. The use of InSAR to detect crustal deformation is described by e.g. Massonnet and Feigl (1998) and Massonnet and Sigmundsson (1999). Briefly, the phase difference between two satellite images acquired at different times creates an interference pattern that can be used to measure crustal deformation with accuracy at the level of millimeters. A range change (change in the distance from ground to satellite) of 28 mm produces one full cycle of color fringes in an interferogram, for C-band radars such as ERS-1 and ERS-2.

3. Field observations

Our fieldwork began 14 months after the June 4, 1998 earthquake. Therefore, it was important to develop criteria to estimate when the observed surface disruption occurred. Freshness of surface features was assessed qualitatively in the field by observation of unweathered surfaces of broken

Table 1
Precision of earthquake data used in this study

	All events; location precision ± 500 m (%)	All events; location precision ± 1 km (%)	$M \geq 3$; location precision ± 500 m (%)	Number of events per year
1994	6	43	43	4808
1995	8	48	67	8606
1996	14	60	64	4067
1997	45	92	94	16256
1998	37	88	80	17059

rock free of lichen and moss, plant roots exposed around where stones had fallen, plant matter not yet decomposed or only partially decomposed under fallen stones, and bare rock surfaces and/or fresh soil exposed when vegetation had been torn away.

Most surface effects were observed to the west and north of the uplift center. To the north, deformation consists primarily of rockfall, bank collapse, and slope failure. To the west, deformation is more severe and includes rupture through soil and bedrock, widening of old fractures, formation of sinkholes, shattering of 'a'a lava, and rockfall from scarps and within fissures. The styles of these surface effects can be classified into several categories (see Figs. 2–4).

3.1. Type A: fresh fractures in soil cover

We observed opening mode cracks, both en echelon and in series, in soil cover up to 1 m thick at two locations (Fig. 2, photo 2 and locations marked A), approximately 2 km north-northeast and 2.5 km northeast of the epicenter of the June 4, 1998 earthquake. The fracture segments are up to 1.5 m wide and up to several meters long, but most are no more than 2 m in length. Shorter segments are found most often at the tips of longer segments. Because our measurements were made 14 months after the earthquake, we were not able to accurately determine the original width of opening. Erosion has widened the surface of the rupture and soil has slumped into the open cracks so that the surface width is not truly representative of the amount of opening. At the bottom of some segments, maximum opening of 1.06 m was measured between bedrock walls below the soil cover. These ruptures are best exposed in the bare soil areas, where vegetation is scarce.

3.2. Type B: fresh rockfalls in old fissures

Along many fault segments on the Bitra lava platform (Sæmundsson, 1995), blocks of columnar jointed basalt up to 1 m in diameter have fallen from the fracture walls into piles at the bottom of the fissure (Fig. 3, photo 1 and locations marked B). We were not able to determine whether the fractures have actually widened at depth or whether rockfalls are the result of ground shaking from movement on a nearby fault. If widening occurred at depth, it must have been small and not detectable at the surface. The largest pre-existing fracture mapped on Bitra (Fig. 2, white dotted line on air photo) is 2.3 km long and extends almost the entire N–S length of the lava platform. However, rockfall is concentrated only at the northern end of this fracture, just south along strike from the above-described fresh fractures in soil cover (see 3.1. Type A: fresh fractures in soil cover). Deformation is minor at the southern end of the Bitra fracture, and largely absent in the central part. Type B deformation is also found on the southeastern part of the Bitra lava platform, close to the center of volcanic uplift (Fig. 3).

3.3. Type C: fresh rockfalls on old scarps

Steep scarps bounding predominantly N-trending valleys have experienced recent rockfalls (Figs. 2 and 3). Large blocks have broken away from bedrock outcrops at the top of the scarp. Along some scarps, rocks have been loosened from the soil but not yet fallen completely. The gap between rock and bare soil is commonly on the order of centimeters, and recently broken plant roots can be seen at the edges of the turf around the loosened rock. Along the scarp on the western edge of Bitra, soil-covered talus is commonly torn in linear gashes between outcrops where rockfall has occurred. These linear tears support the hypothesis that rockfalls were a result of either motion on this fault, which lies along the trend of aftershocks from the June 4, 1998 earthquake, or from seismic shaking. Although we cannot determine definitively which of these processes is responsible, we are confident that rockfall was not a result of water erosion. Similar tears were not observed on vegetated scarps farther from the epicenter. The largest rockfalls occurred on the steepest, most unstable slopes in the northeastern part of the area, up to 6 km from the epicenter. However, the greatest concentration of rockfall occurred in the E–W-trending Kýrgil gorge, which

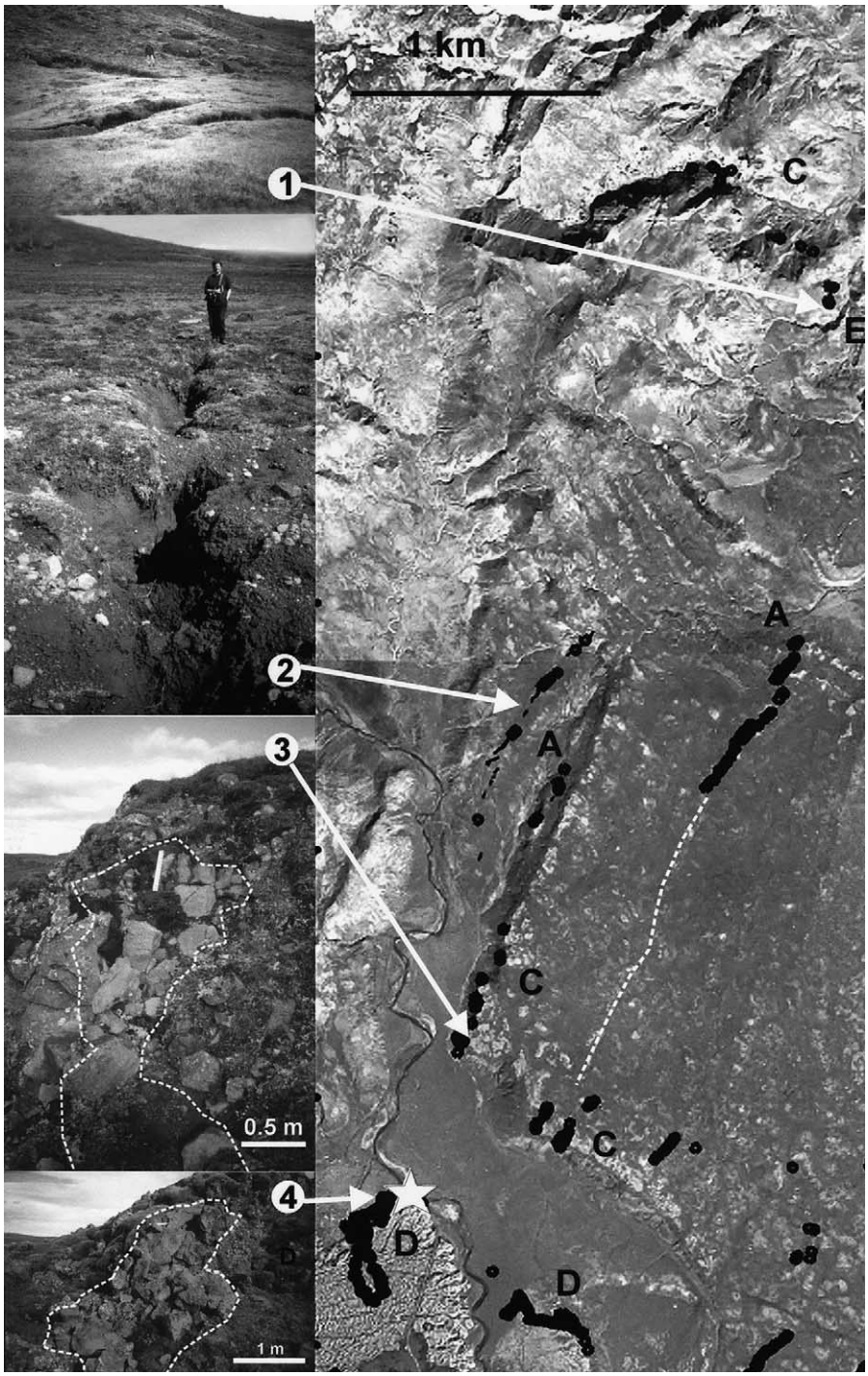

Fig. 2. Close-up image of area along strike from the epicenter of the June 4 earthquake (white filled star). Letters on air photo refer to types of surface effects described in 3. Field observations. Black points and lines on air photo are locations where surface effects were mapped. Dotted white line shows trace of longest fault on Bitra lava platform.

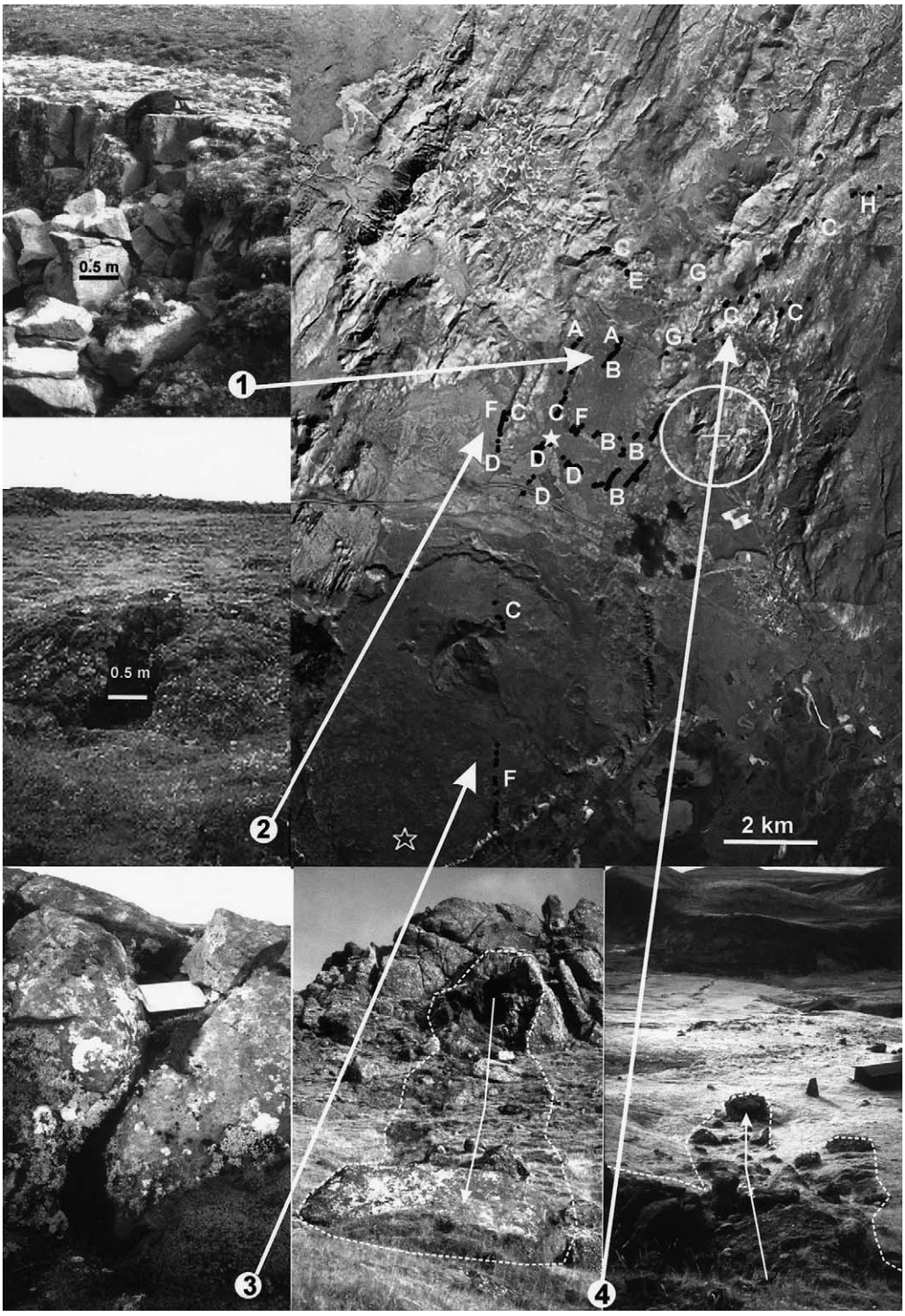

Fig. 3. Surface effects mapped in study area (black points and lines). White circle denotes center of volcanic uplift. Letters on air photo refer to types of surface effects described in 3. Field observations.

lies along the trend of aftershocks from the June 4, 1998 earthquake, approximately 4 km north of the epicenter.

3.4. Type D: freshly broken blocks of 'a'a lava

Freshly broken blocks of lava were observed in 'a'a flows in three main locations (Fig. 2, photo 4 and locations marked D). They were first seen in a flow that lies immediately south of a NNE-trending normal fault scarp (marked LSM in Fig. 1). Here a line of broken lava follows the same trend as the scarp and corresponds to the geometry of fringe discontinuities observed by In-SAR and interpreted by Feigl et al. (2000) as resulting from 7 mm of aseismic down to the west dip-slip. Its presence on the interferogram guided the field search here for surface effects. The 2000-yr-old lava flow is covered in thick moss, but jagged projections of lichen-covered lava protrude above the moss. Pieces of broken rock range in size from a few centimeters to more than 1 m in diameter. Most breaks are shorter than 1 m and are commonly spaced several meters apart. At the toe of this part of the flow, elongated linear depressions in the turf have been observed. Such grass-covered sinkholes are characteristic of old faults in Iceland (for further discussion see 3.7. Type G: opening or widening of sinkholes) so that their presence here suggests that the disrupted 'a'a lava falls along the trace of an old fault.

The epicenter of the June 4, 1998 earthquake (Árnadóttir et al., 1999) is located approximately 1 km to the east, at the front of the above-mentioned lava flow. Here disruption of the lava is much more dramatic, obvious and pervasive. In places, the whole pile of lava appears to have been uplifted, exposing fresh soil at its base. Broken blocks at this location look as though they have been forcibly shattered (Fig. 2, photo 4). This part of the flow is thicker than it is to the north and the flow front is steep and lobate. Broken pieces of lava are also much larger and more closely spaced, and seem to occur more commonly in the 'channels' between lobes at the flow front (Fig. 2, see area of highest point density marked D). At least two of these channels end at grass-covered sinkholes in the turf (see above and 3.7. Type G: opening or widening of sinkholes) which extend along strike to the north of the flow front, suggesting the possibility that the lava originally flowed into a pre-existing fissure.

3.5. Type E: landslides

Approximately 4 km to the north-northeast along strike from the epicenter of the June 4, 1998 earthquake, at Kýrgil, slope failure occurred along a series of en echelon tears in the turf (Fig. 2, photo 1 and location marked E) affecting a 1000-m^2 area. Large rocks also fell from the steep outcrop above the slope. Fresh scars in the outcrop indicate that the falls were recent. Further landslide deposits were described approximately 1.5 km north of this location (K. Sæmundsson, pers. commun., 1999). Reactivation of an older landslide occurred from the top of a very steep scarp at the eastern end of the E–W-trending Kýrgil gorge. This slide is clearly visible on 1991 air photos. Fresh fractures were observed in soil at the head of the slide. Plant roots were torn from the ground and large blocks of freshly broken bedrock with unvegetated surfaces had fallen from the outcrop below the soil. Little evidence of water erosion was observed and reactivation appears to have affected only the top of the slope. The fact that this slide occurred during the summer and along the trace of aftershocks from the June 4, 1998 earthquake supports the conclusion that either shaking or fault movement caused the slide.

3.6. Type F: loosened push-up structures

In three separate locations (Fig. 3, photos 2 and 3 and locations marked F) piles of lava blocks are arranged along a N–S trend. These are interpreted as pre-existing compressional push-up structures characteristic of many strike-slip faults in the SISZ (e.g. Bjarnasson et al., 1993). Field evidence suggests that many of the lava blocks within the push-ups have recently been rotated and loosened from their original position, indicating possible reactivation of an underlying fault. Gaps between

rock and soil range in width from millimeters to several centimeters and expose fresh soil and newly torn plant roots. In a few cases, rock is freshly broken. It is difficult to decide whether type F deformation is a result of the earthquakes or attributable to frost action. Frost action can lift large blocks out of the soil, but it is doubtful that the observed rotation would also occur. The fact that these locations are in close proximity to known earthquake epicenters and that they lie along previously mapped faults suggests that fault movement is the more likely cause. The southernmost occurrence of type F deformation, on the lava shield Skálafell, is also coincident with deformation seen on co-seismic interferograms we examined (see 7. SAR interferograms) which indicate that this fault was active during the June 4, 1998 earthquake.

3.7. Type G: opening or widening of sinkholes

Linear or aligned circular sinkholes are characteristic of many old, soil-covered fractures in Iceland (P. Einarsson, pers. commun., 1999). Such grass-filled depressions are common in the study area, particularly in the vicinity of mapped faults on the Bitra platform. These are assumed to be remnants of gashes formed in the soil (described in 3.1. Type A: fresh fractures in soil cover) which have subsequently been filled in by erosion and covered with vegetation along the sides and bottom of the depression. Some of these older, vegetated sinkholes show ambiguous evidence of recent re-opening, e.g. torn grass in the bottom exposing fresh soil. Sinkholes were also observed (Fig. 4, photo 2 and locations marked G), along two hyaloclastite ridges bracketing the Ölkel-

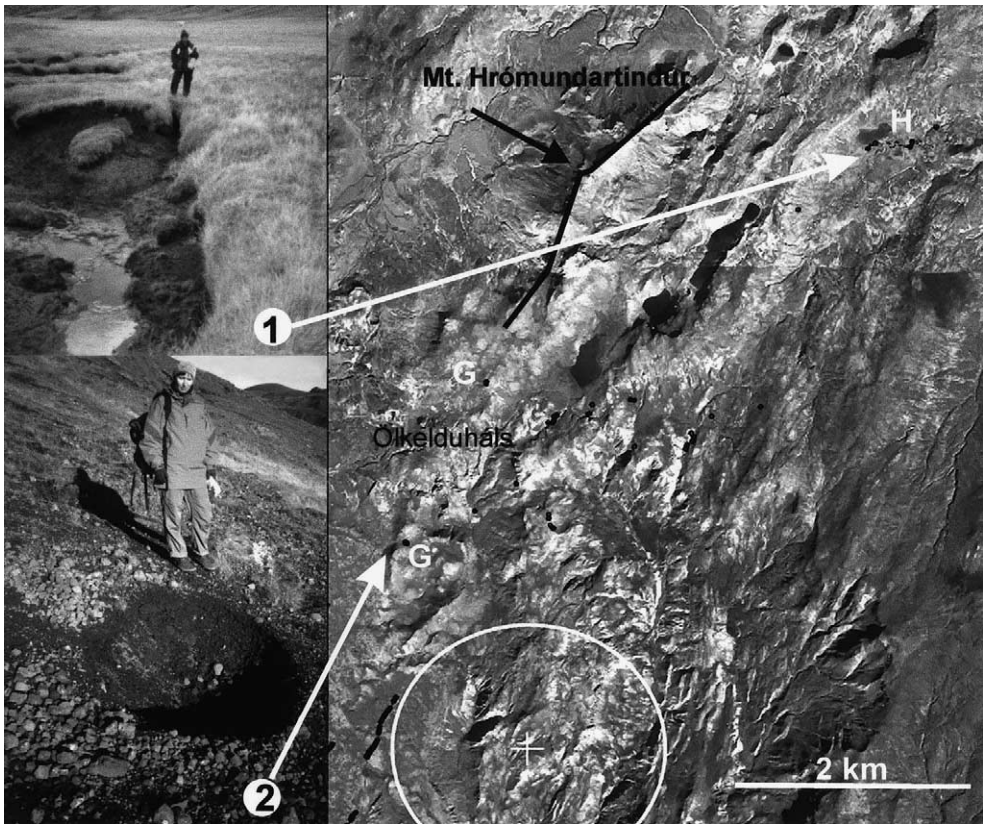

Fig. 4. Close-up of surface effects to the northeast of epicenter. White circle denotes center of volcanic uplift. Letters on air photo refer to styles of surface effects described in Section 3. Field observations. Black points and lines on air photo are locations where surface effects were mapped. Thick black line shows axis of Mt. Hrómundartindur.

duháls geothermal area. Torn vegetation and freshly exposed soil and bedrock were observed in three sinkholes north of Ölkelduháls, up to 3 m in diameter and more than 2 m deep. These sinkholes are visible on the 1991 air photos, aligned along a NNE-trending linear depression on the lower slopes of Mt. Hrómundartindur. Although erosion cannot be discounted as the cause of the torn vegetation and exposed soil, an interpretation of reactivation is favored for the following reason. Directly south of Ölkelduháls and along strike from the aforementioned sinkholes, four freshly opened sinkholes were first observed during a GPS campaign in August, 1998 (Hreinsdóttir, 1999). They occur in bare soil on the side of a steep slope and have sharp, well-defined edges which could not have resulted from slope erosion. Rather they must have been caused by opening of a fracture in the underlying bedrock. Although they do not lie over a noticeable lineament or mapped fault, they are aligned parallel to the strike of the hyaloclastite ridge on which they sit, as well as parallel to other fractures which cross the geothermal area. Because these two sets of sinkholes lie along strike from each other on either side of the active geothermal area and are within 2 km of the uplift center, we suggest that they were opened by inflation of the area and/or reactivation (or shaking) of an underlying fault that runs through the hyaloclastite ridges.

3.8. Type H: bank collapse

In a valley 1.5 km east of the northern end of Mt. Hrómundartindur, a bank has collapsed

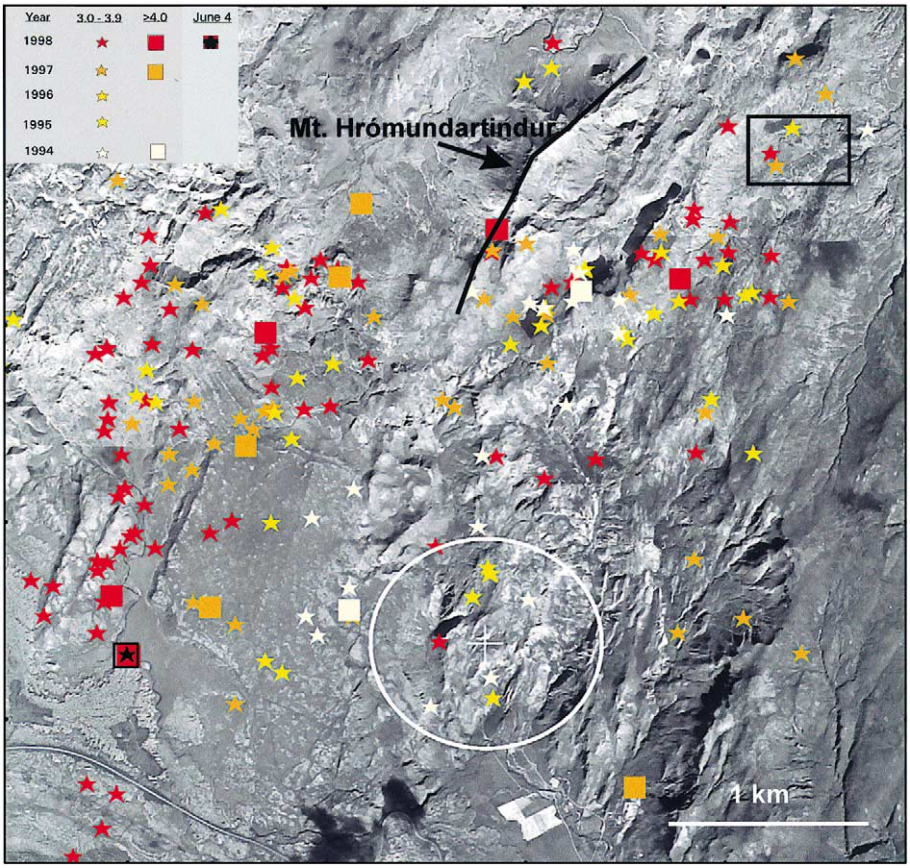

Fig. 5. Earthquakes $M_L \geq 3.0$ to the north and west of the uplift center (white circle) between 1994 and 1998. Red square with black star is epicenter of June 4, 1998 $M = 5.1$ earthquake. Black box shows area of bank collapse discussed in 3.8. Type H: bank collapse. Thick black line shows axis of Mt. Hrómundartindur.

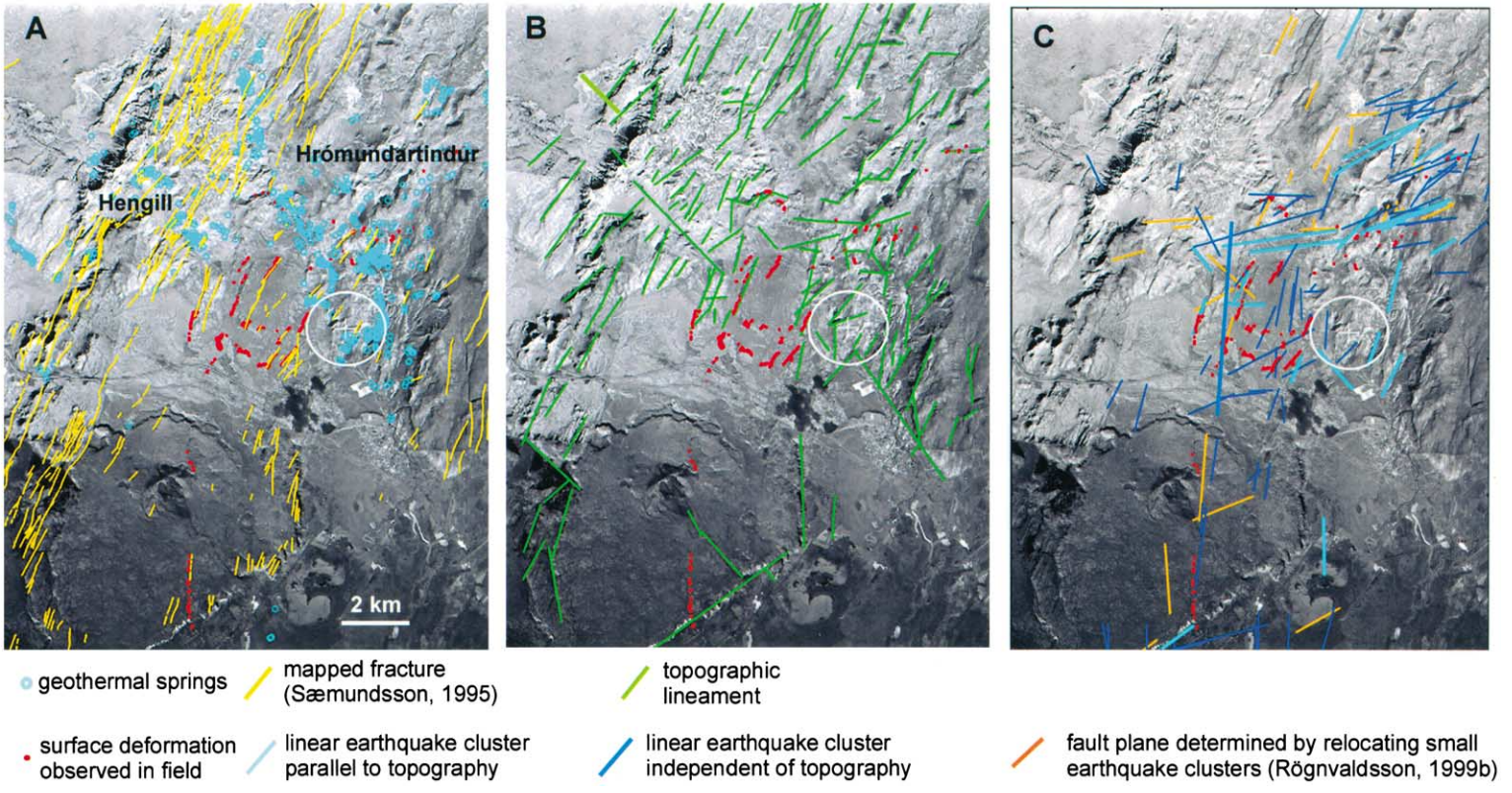

Fig. 6. (A) Faults and geothermal springs. (B) Topographic lineaments. (C) Earthquake lineaments. Field data shown in red. Uplift center shown as white circle.

along a very straight, 500-m-long E–W-trending stretch of a stream channel (Fig. 4, photo 1 and location marked H). Observed bank collapse at this location was pervasive and appears to be the result of a single event. Thick soil along the steep sides of the channel is slumped down and large pieces of turf are torn from the bank. It is difficult to say with certainty whether this event resulted from seismic shaking or if it was simply a result of flooding. There are two reasons in favor of an interpretation of seismic shaking. If the bank collapse was due to flooding, it is likely that the soil would have been washed away rather than remaining in situ. The very straight geometry of the channel and its orientation along an E–W trend coincide with other structural elements in the study area, including E–W-trending faults identified by relocation of small earthquakes (Rögnvaldsson, 1999). Up to 15 earthquakes with $M_L \geq 3.0$ occurred in this valley between 1994 and 1998 (Fig. 5, area enclosed in small box) and one event with $M_L = 3.4$ and a depth of 2 km occurred along or within meters of the stream channel just hours before the large earthquake of June 4, 1998. Therefore, bank collapse due to co-seismic shaking, or perhaps even fault movement below the stream channel, is a reasonable explanation.

4. Topographic lineaments

Faults and fissures are apparently scarce around the Hrómundartindur volcano, in stark contrast to the numerous fissures and faults extending through Mt. Hengill (see Fig. 6A; Sæmundsson, 1967, 1995). However, the pattern of seismicity around Hrómundartindur between 1994 and 1998 indicates that many earthquakes probably occurred on pre-existing weaknesses in the crust. In the active rift zones of SW Iceland rift-related structures, including normal faults, opening-mode fractures and eruptive fissures, have predominant trends between 030° and 045°. NW-trending cross-structures are found only rarely (Sæmundsson, 1979). Along the SISZ (transform), left-lateral strain is accommodated primarily along many subparallel, N- to NNE-trending, right-lateral strike-slip faults and minor E–W-trending conjugate faults experiencing left-lateral motion (Einarsson, 1991). Águstsson (1998) confirmed that all of these trends are reflected in the topography of the Hengill triple junction.

We traced the trend of all relatively continuous, aligned linear or curvilinear topographic features directly over the photomosaic base (Fig. 6B) and generally confirmed the same range of azimuths obtained by Águstsson (1998). However, we note a change in the average trend of lineaments across the area. Around Mt. Hengill, topographic lineaments trend predominantly NE, reflecting their rift-related origin. A single, large NW-trending cross-structure is prominent in the center of the Hengill volcano, and defines a connection from Hengill to the Grensdalur system through the Ölkelduháls geothermal field (Ívarsson, 1998). Faults with this trend are believed to focus much of the geothermal activity east of Hengill (Ívarsson, 1998).

In contrast, topographic lineaments around Mt. Hrómundartindur are much more complex. Structures with a rift-related trend are much less common, whereas N- to NNE-trending structures related to the transform occur more frequently. Short E–W-trending lineaments are also more common. These trends intersect particularly in the area around the Ölkeldúhals geothermal field. Structures with an intermediate NNE trend are more common in the area to the north of Ölkeldúhals.

5. Earthquake distribution

Once in the GIS database, earthquake locations from 1994 to 1999 were plotted directly over the photomosaic according to attributes such as depth, magnitude and date (Fig. 7). From the start of enhanced seismicity, three characteristics became apparent. Firstly, the earthquakes occurred in linear clusters, secondly, most were located either north or west of the uplift center, and thirdly, clusters have a predominantly ENE or N–S trend. Within a 1-km radius of the point source of uplift, the earthquake density was rela-

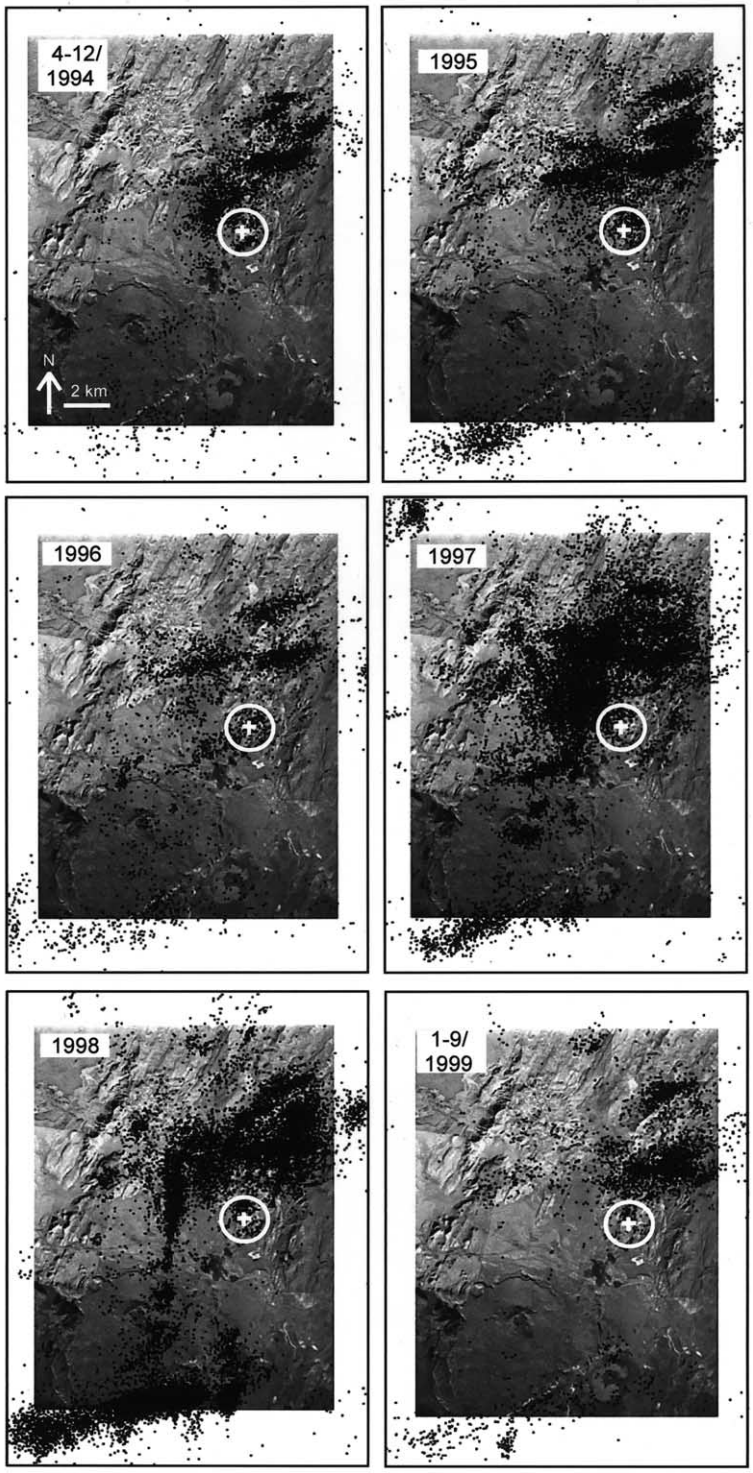

Fig. 7. Distribution of earthquakes between 1994 and 1999. Uplift center shown as white circle in all images.

tively small but constant. Until 1998, most earthquakes in the southern part of the area were confined to the southwestern corner of the small lava shield, Skálafell. With the exception of a small, mostly N-trending cluster in 1997, very few earthquakes occurred southeast of the uplift center. The greatest increase in earthquake activity occurred in 1997. This increase was coincident with a shift in distribution slightly to the west and south of the uplift center. Diffuse clusters of small events started to occur along the trend of the main fault that eventually failed on June 4, 1998, and activity in the south began to align more clearly along an ENE trend in the area of the coming intense swarm of November 13, 1998. In 1998, activity in the center of the region converged onto the June 4 fault and ceased almost completely between there and the uplift center. The earthquake pattern in the north remained relatively stable in location, but decreased in number during 1999, while activity elsewhere had all but ended.

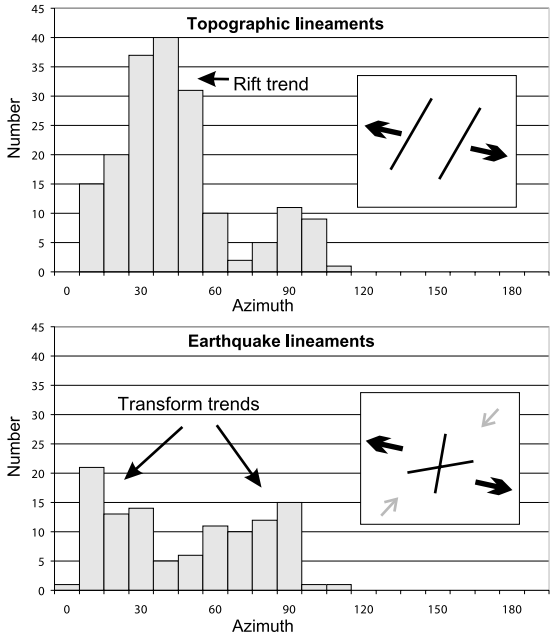

Fig. 8. Histograms of strike for topographic and earthquake lineaments. Inset boxes show schematic diagrams of structures and stress directions responsible for their formation.

6. Earthquake lineaments

Many of the earthquakes at Hengill during the period 1994–1998 occurred in linear clusters whose average half-width is about 200 m. We plotted earthquake locations month by month in map view and drew lines manually through the central axes of 115 apparently linear clusters. Approximately 30% of clusters are parallel to nearby (within 200 m) topographic features (Fig. 6C, lines in light blue). Histograms of the strike of topographic and earthquake lineaments show generally the same range of azimuths. Whereas most topographic lineaments strike in the rift direction (NE), earthquake clusters fall predominantly along transform-related trends (Fig. 8). N-trending clusters are more common west of the uplift center and E–W-trending clusters are more common north of the uplift center. Although mapped faults are rare in those areas, both earthquakes and topographic lineaments suggest their presence. Relocated fault planes (Rögnvaldsson, 1999), shown in orange (Fig. 6C) confirm that E–W structures were active, especially north of the uplift center in the most active geothermal areas.

7. SAR interferograms

We use the same series of interferograms used by Feigl et al. (2000) to evaluate deformation associated with the earthquakes. Four interferograms in our dataset span the June 4, 1998 earthquake. Of the four co-seismic interferograms available, only two have enough coherence to allow any interpretation and, even on these, the coherent area is small, making modeling difficult. Two sets of concentric fringes on the pre-seismic interferogram show an uplift signal more or less symmetric about a central area (Fig. 9C). The fringes straighten out along a N–S trend in the southernmost part of the interferogram, suggesting that aseismic slip along a N-trending fault may have occurred before the June 4 event. Both co-seismic interferograms (A and B) show that the uplift signal has been strongly perturbed or overprinted by deformation related to the

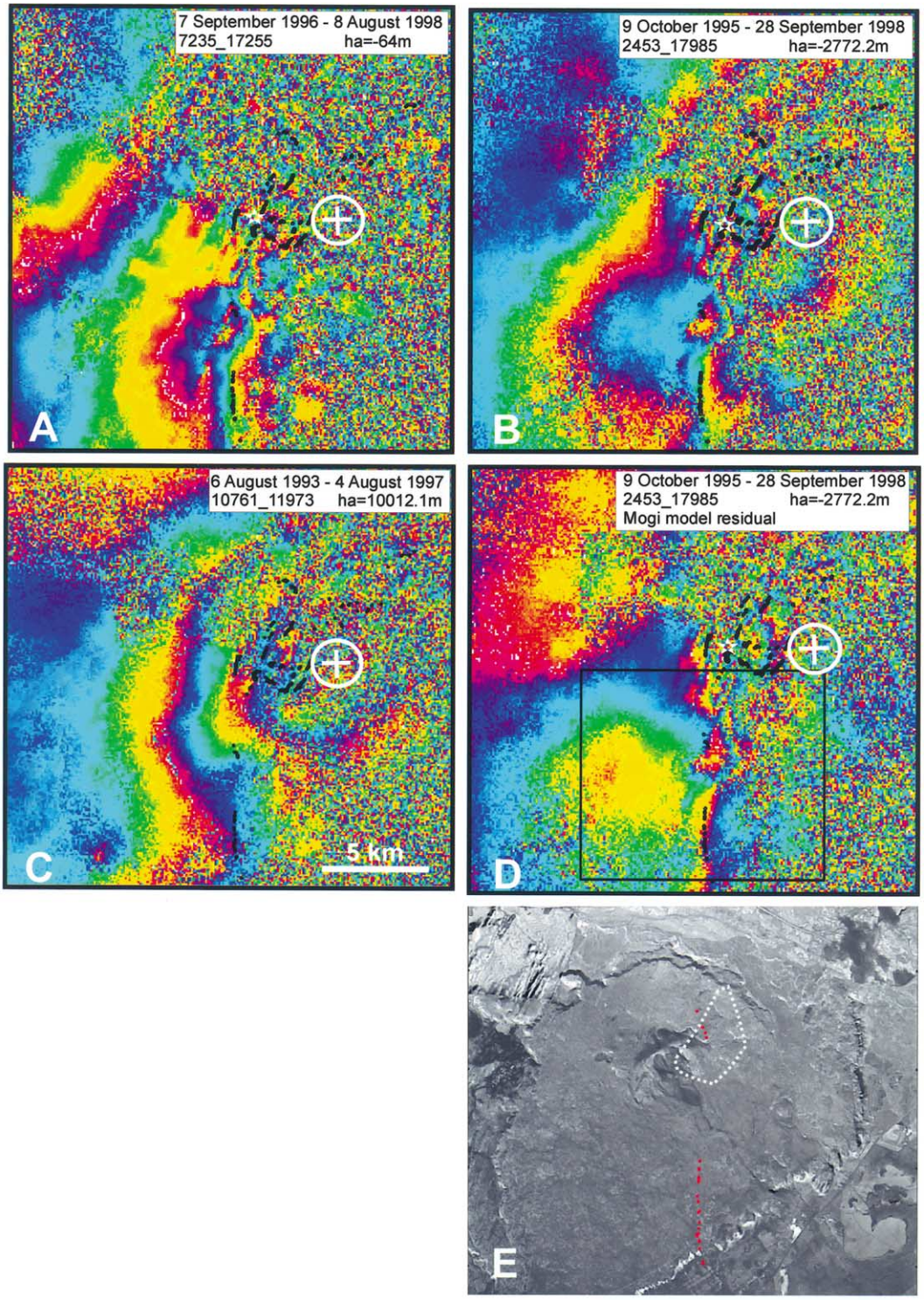
7 September 1996 - 8 August 1998
7235_17255 ha=-64m
A
9 October 1995 - 28 September 1998
2453_17985 ha=-2772.2m
B
6 August 1993 - 4 August 1997
10761_11973 ha=10012.1m
C
5 km
9 October 1995 - 28 September 1998
2453_17985 ha=-2772.2m
Mogi model residual
D
E

$M_L = 5.1$ earthquake. The uplift signal, while barely visible to the east of the epicenter, has been offset slightly to the southwest of the original uplift center and a large central area has been flattened out. The area of coherence begins just south and to the west of the epicenter, where linear fringes can be seen striking NE (029°). South of there a prominent semi-circular area of fringes can be seen on the northern slope of Skálafell. Assuming that all motions are vertical, these indicate relative subsidence of a 3.1-km^2 area (white dashed line in Fig. 9E) bounded on the west by a steep NE-trending gradient in the fringes. Continuing south, the most prominent signal on the interferogram is a set of N–S-trending fringes which fall along the trace of a previously mapped fault, and coincides with type F deformation observed at the surface.

We used an elastic half-space model of a Mogi point source to remove the deformation signal resulting exclusively from volcanic uplift and produced a residual image (Fig. 9D) that shows only co-seismic deformation. The linear discontinuity on the south slope of Skálafell and the semi-circular area of subsidence on the north slope are the most prominent features on this interferogram. In addition, a broad, dome-like uplift signal can be seen on the west side of the image. The linear fringes indicate 16 mm of subsidence from west to east across the fault over a distance of 1500 m.

8. Summary and discussion

Field data alone suggest that most, if not all, of the surface effects observed during this study have occurred along pre-existing faults, many of which were previously unmapped. Lines of evidence include the presence of grass-covered sinkholes along strike from fresh surface rupture, the opening of fresh rupture along strike from mapped faults, and the opening of sinkholes along topographic lineaments. The spatial correlation of topographic lineaments and earthquake lineaments (Fig. 6C) supports the hypothesis that local topography often results from underlying (buried) fault planes. Relocated earthquake fault traces (Rögnvaldsson, 1999) are also commonly parallel to topographic lineaments and provide further support for buried faults. Most surface effects occurred along NE- and NNE-trending structures, but some disruption was observed along E–W-trending structures (Figs. 6C and 10). Short, E–W-trending topographic lineaments lying between N- and NNE-trending ridges are common in our field area (Figs. 6B and 10). Their correlation with earthquake lineaments and relocated fault planes suggests that they are more important for accommodating strain than has been previously thought. This fault geometry is consistent with an E–W-trending shear zone.

Surface effects were most intense in the area between the center of uplift and the epicenter of the June 4, 1998 earthquake (both shown in white in Fig. 10) and decreased significantly to the south along the trace of aftershocks. The number of aftershocks also decreased towards the south, and two apparent gaps in the aftershocks can be seen on Skálafell (white arrows in Fig. 10) where surface effects were minor. Aftershocks there occurred at a much shallower depth (see Fig. 11A) than those closer to and north of the epicenter, except within the circular cluster of events between the aftershock gaps. Here, four aftershocks at depths between 8 and 12 km and one at depth > 12 km occurred. In addition, eight of these events had $M \geq 3$ (see Fig. 11B). This cluster is coincident with the semi-circular depression seen in the co-seismic interferograms (Fig. 9D) and with a gentle, but significant break in slope on Skálafell.

Little or no evidence of rupture was observed around the intense earthquake swarm of Novem-

Fig. 9. (A) 2-yr co-seismic interferogram. (B) 3-yr co-seismic interferogram. (C) 4-yr pre-seismic interferogram. (D) 3-yr co-seismic interferogram residual after removing Mogi source. (E) Air photo close-up of Skálafell. Area enclosed by dashed white line is same as areas of subsidence on interferograms (B)–(D). Field data shown in black in (A)–(D) and in red in (E). Epicenter of June 4, 1998 earthquake shown as white star. Box in (D) shows area covered in photo (E).

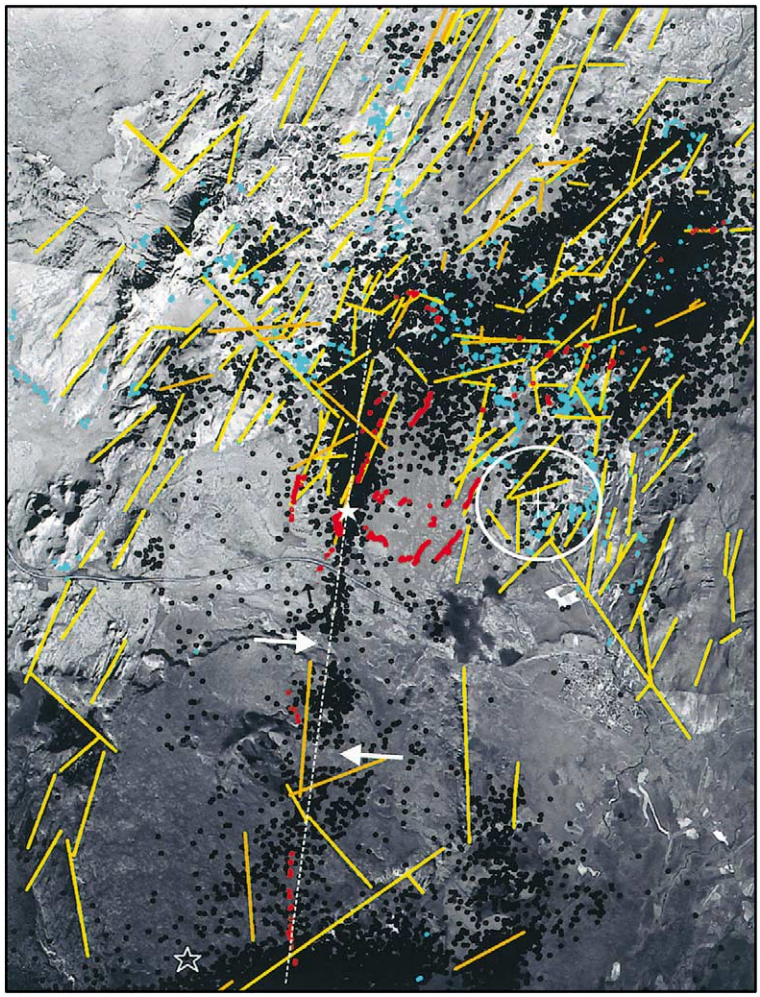

Fig. 10. Figure summarizing structural complexity of the study area. Black points are earthquakes for 1998; yellow lines are topographic lineaments; blue circles are geothermal springs; red points are mapped surface effects; orange lines are relocated fault planes (Rögnvaldsson, 1999). Dashed white line shows trace of aftershocks from June 4, 1998 earthquake. White arrows point to gaps in the line of aftershocks.

ber 13, 1998, in spite of the number of events with $M \geq 3$. Here, aftershocks deepen, and more large events occur at the southwest end of this zone (Fig. 11B). However, the only observation of surface disruption in this area was minor rotation or loosening of a few stones, too ambiguous to map.

In the weeks prior to the June 4, 1998 earthquake, a network of 20 GPS stations had been measured in the area. After the earthquake, the network was partly remeasured (Thorbergsson and Vigfusson, 1998). These data, reprocessed by Hreinsdóttir et al. (2001), suggest that about 19.4 cm of N–S-oriented, right-lateral strike-slip movement occurred between the two nearest GPS stations (Fig. 12). Vertical changes of about 15 cm occurred across the fault trace, down to the west. The geodetic stations are located just north of the main shock epicenter. A dislocation model of this motion by Árnadóttir et al. (1999) using the co-seismic GPS data suggests that approximately 28 cm of right-lateral strike-slip, 15 cm of dip-slip and 3.2 cm of opening have occurred. We attempted to apply this model to our co-seismic interferogram, but the fit was not good. Un-

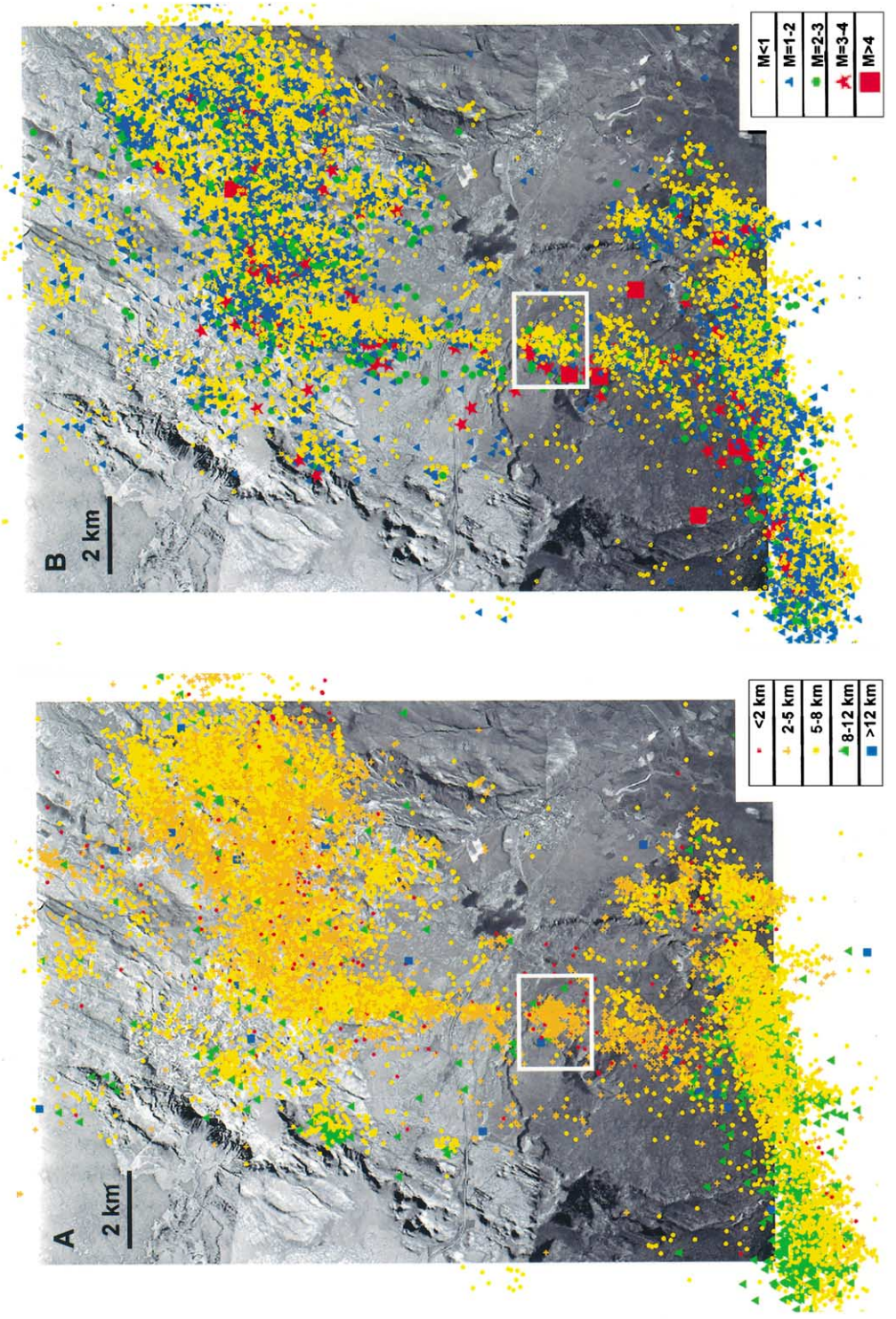

Fig. 11. Earthquakes in 1998: (A) plotted by depth; (B) plotted by magnitude. White box marks area where subsidence has occurred.

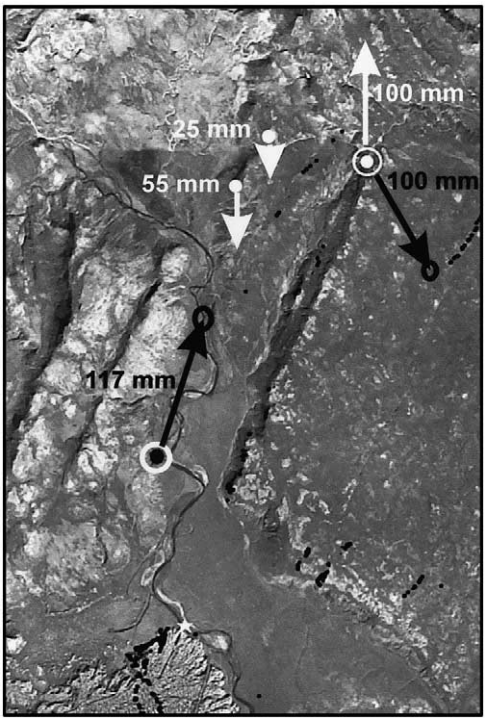

Fig. 12. GPS and leveling data from Thorbergsson and Vigfusson (1998) reprocessed by Hreinsdóttir et al. (2001). Points shown in white are leveling points. Points enclosed in white circle are GPS points. White arrows show vertical displacements. Black arrows show horizontal displacements. Black circles show 95% confidence region for horizontal measurements. All motion is calculated relative to a permanent GPS station in Reykjavik (approximately 35 km to the west).

fortunately, the southern part of the rupture is not well constrained by the GPS data, since all of the stations are located north of Skálafell. However, both the interferograms and our field data indicate that slip must be smaller at the southern end than at the northern end of the fault that failed in this earthquake.

The field, lineament and seismic data presented here support the conclusion that strain around the center of uplift during the period 1994–1998 was accommodated primarily along pre-existing weaknesses in the crust. As the Hrómundartindur volcanic system slowly moved off-rift, faults and fissures that formed on axis were buried by younger lava flows and alluvium, while mostly inactive fault scarps eroded. The well-developed fissure swarm of the Hengill system now accommodates the extensional strain from rifting, while the older fractures at Hrómundartindur remain as buried conduits for geothermal fluids. At the same time as the Hrómundartindur system moved off axis, it drifted into the stress field of the SISZ (transform). Both fault and lineament maps (Fig. 6A,B) show that the NE-trending structures of the rift zone intersect N-trending structures of the SISZ in the central part of our study area. This area of greatest strike variability coincides with the area of greatest earthquake density. There are many structures with a NNE trend around the Hrómundartindur system that may be a result of rotation of northeastern structures as the system came under the influence of the transform. These faults, particularly the one that failed on June 4, 1998, must have been close to failure when movement was triggered by magmatic inflation (Sigmundsson et al., 1997; Feigl et al., 2000). It may be that seismic activity at Hrómundartindur marked the beginning of a new earthquake cycle in the SISZ. It was followed in February 2000 by an eruption of Hekla, at the eastern end of the SISZ, and then two $M \geq 6.6$ earthquakes occurred in the center of the seismic zone on June 17 and 21, 2000.

Sigmundsson et al. (1997) showed that a pressure source at depth embedded in an area experiencing left-lateral horizontal shear will enhance shear in quadrants to the northeast and southwest, radiating from the center of the pressure source. When added to the regional stress, it is sufficient to trigger faulting. In this model, the effect of confining pressure on friction on faults was not considered. Feigl et al. (2000) calculated the Coulomb stress change due to a volume change in a Mogi source at the center of concentric fringes on interferograms. The Coulomb stress change was calculated on optimally oriented faults, with strike that maximized the Coulomb stress. The effect of a regional stress field was included, assuming that σ_1 is horizontal and oriented NE–SW, σ_3 is also horizontal and oriented NW–SE (e.g. Sæmundsson, 1978) and the stress magnitude was set at 1 bar. These results show that earthquakes should occur within an area elongated in a NE–SW direction around the uplift

center (Feigl et al., 2000, see their plate 3a), with a positive stress change greater than 2 bar, favoring motion along N–S-trending right-lateral strike-slip faults. With the revised location of the pressure source by Feigl et al. (2000), earthquake hypocenters were offset to the northwest of the source and were notably absent in more than half of the area of stress increase. The authors note that, instead, earthquakes seem to concentrate in an area that coincides with a V_P/V_S anomaly related to hydrothermal alteration (Miller et al., 1998), and conclude that the shape of this anomaly is a result of a zone of alteration around the faults and fissures that act as conduits for hydrothermal fluids. This anomaly does not extend to the smaller geothermal area in Hveragerði, south of the uplift center, which may partially explain the lack of seismicity there. In spite of the presence of many N-trending faults in the Grensdalur volcanic system, relatively few earthquakes occurred there during the 1994–1998 period. We suggest that this focusing of activity to the north and west of the uplift center reflects that in this area the crust was most ready to fail, due to the combined effects of hydrothermal alteration and the intersection of rift and transform-related structures.

InSAR and geologic data suggest that the geometry of the fault that failed on June 4, 1998 is more complicated than the straight line of aftershocks first indicated (Fig. 13). Modeling of deformation due to faulting has proven difficult due to the change in character of the signal from south to north. The strike of major structures changes from N to a more NNE trend, indicating that the fault is segmented in nature. Fringes on the interferogram, topographic lineaments, previously mapped faults and earthquake clusters all show that structures change in strike north of the Skálafell lava shield. Mt. Hrómundartindur itself exhibits such a right bend north of Ölkelduháls (see black line in Fig. 5). Such geometry is to be expected at a triple junction where N-trending structures related to the SISZ transform intersect NE-trending structures related to rifting. The semi-circular depression seen in interferograms over the northeast slope of Skálafell may be a result of slip along a low-angle fault at shallow

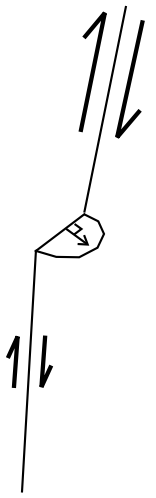

Fig. 13. Proposed model of fault geometry. Fault strike is not well constrained. Southern fault segment is sub-vertical and strikes between 000° and 005°. Northern segment, also sub-vertical, could strike anywhere between 000° and 029°. Model shows right-lateral strike-slip, with greater slip on the northern fault segment. Right bend at segment boundary produces local subsidence along a shallow, low-angle dip-slip fault, consistent with the focal mechanism of the largest aftershock on June 4, 1998.

depth. Subsidence of this type would occur at a segment boundary along a right-lateral strike-slip fault when a right bend or a right step is present between adjacent fault segments. The largest aftershock on June 4, 1998 ($M_L = 4.6$) occurred in this area. The focal mechanism of this event is consistent with normal movement on a fault striking N63°E, dipping 42°E at a depth of 3.1 km (Kristín Vogfjörð, personal communication, 2001). Preliminary modeling shows that approximately 5 cm of dip-slip on a buried low-angle fault can produce a set of circular fringes similar to what we see on the interferogram. The east-facing slope on the north summit area of Skálafell is unstable and appears to have experienced an unknown number of landslides in the past. It is likely that landslides here have resulted from previous earthquakes at this location.

Earthquakes with $M \geq 3$ (see Fig. 5) occurring in the geothermal area north of the uplift center remained in the same locations, whereas earthquakes to the west of the uplift center migrated westward through time until strain converged on

the fault that finally failed on June 4. We suggest that the earthquakes were migrating westward in response to continued uplift until slip was triggered on a fault. Small earthquakes that occurred in 1997 along the trend of the coming $M_L = 5.1$ earthquake were precursory to that event. Most of the surface effects we observed were concentrated in the region between the center of uplift and the epicenter of the June 4, 1998 earthquake. All of our data indicate that slip along the June 4 fault was not uniform, but decreased substantially towards the south. The decreasing severity of surface effects away from the epicenter of the June 4, 1998 $M_L = 5.1$ event suggests that this event was the primary cause for the observed surface effects.

9. Conclusions

The geologic and geophysical data presented here support the conclusion that strain resulting from volcanic uplift under the Hrómundartindur volcanic system focused in the area of greatest structural complexity to the north and west of the center of uplift. Here, the N- and E-trending structures from the SISZ transform intersect the NE-trending structures related to rifting. Additional crustal weakness is due to alteration of the crust above the Ölkelduháls geothermal system. Earthquakes migrated westward as uplift proceeded until strain converged onto the fault that finally failed on June 4, 1998. We conclude that most, if not all, of the surface effects observed are likely due to the June 4, 1998 earthquake. Interpretation of interferograms in combination with field data suggests that distributed slip occurred along a right-stepping or right-bending, segmented right-lateral strike-slip fault.

Acknowledgements

Support for this work was provided by a U.S. Fulbright Fellowship, NSF Fellowship (EAR-9901486), and European Community contract ENV4-CT97-0536+A6 (PRENLAB-2 project). We are grateful to Rósa Ólafsdóttir for the work she did in ArcInfo. We thank Páll Einarsson for assistance in early stages of the fieldwork, and Kristján Sæmundsson for advice, discussion and review of the manuscript in its early stages. Mackenzie Johnson, Rikke Pedersen, Peter Momme, Daniel Larson, TorSigvald Johanson, Rósa Ólafsdóttir and Anna Eiriksdóttir provided assistance with the fieldwork. Thomas R. Walters and Roland Bürgmann are thanked for constructive reviews.

References

Águstsson, K., 1998. Stefnur og strik í landslagi á Hellisheiði og í Hengli. Verðurstofa Íslands Greinargerð, VÍ-G98037-JA095.

Árnadóttir, Th., Geirsson, H., Bergsson, B.H., Völksen, C., 2000. The Icelandic continuous GPS network – ISGPS: March 18, 1999–February 20, 2000. Icelandic Meteorological Office Report VÍ-R00002-JA02.

Árnadóttir, Th., Rögnvaldsson, S., Águstsson, K., Stefansson, R., Hreinsdóttir, S., Vogfjörð, K., Thorbergsson, G., 1999. Seismic swarms and surface deformation in the Hengill area, SW Iceland. Seismol. Res. Lett. 70, 269.

Bretar, F., 2000. Mesures tectoniques interférométriques SAR par déformation active: application au volcan Hekla, Islande. Master Thesis, Université Denis Diderot, Paris, 32 pp.

DeMets, C., Gordon, R., Argus, D., Stein, S., 1994. Effect of recent revisions to the geomagnetic reversal time scale on estimates of current plate motions. Geophys. Res. Lett. 21, 2191–2194.

Einarsson, P., 1991. Earthquakes and present-day tectonism in Iceland. Tectonophysics 189, 261–279.

Einarsson, P., Sæmundsson, K., 1992. Earthquake epicenters 1982–1985 and volcanic systems in Iceland (map), in Í Hlutarsins Eðli. In: Th. Sigfússon (Ed.), Festschrift for Thorbjorn Sigurgeirsson. Menningarsjóður, Reykjavík.

Feigl, K., Gasperi, J., Sigmundsson, F., Rigo, A., 2000. Crustal deformation near Hengill volcano, Iceland 1993–1998: coupling between magmatic activity and faulting inferred from elastic modelling of satellite radar interferograms. J. Geophys. Res. 105, 25655–25670.

Foulger, G.R., 1988a. Hengill triple junction, SW Iceland, 1. Tectonic structure and the spatial and temporal distribution of local earthquakes. J. Geophys. Res. 93, 13493–13506.

Foulger, G.R., 1988b. Hengill triple junction, SW Iceland, 2. Anomalous earthquake focal mechanisms and implications for process within the geothermal reservoir and at accretionary plate boundaries. J. Geophys. Res. 93, 13507–13523.

Gasperi, J., 1999. Etude de la déformation lithosphérique par interférométrie radar. Application à la région de Hengill, Islande. Ph.D. Thesis, Université Paul Sabatier, Toulouse, 218 pp.

Halldórsson, P., Stefánsson, R., 1986. Jarðskjálftar á Hengilss-

væði, áhrifamat fyrir Nesjavelli. Unnið fyrir Hitaveitu Reykjavíkur. Veðurstofa Íslands (internal report).

Halldórsson, P., Stefánsson, R., 1987. Jarðskjálftahætta á Geithálsi og við Sog. Unnið fyrir Landsvirkjun. Veðurstofa Íslands (internal report).

Hreinsdóttir, S., 1999. GPS Geodetic Measurements on the Reykjanes Peninsula, SW Iceland: Crustal Deformation from 1993 to 1998. Master Thesis, University of Iceland, Reykjavík, 114 pp.

Hreinsdóttir, S., Einarsson, P., Sigmundsson, F., 2001. Crustal deformation at the oblique spreading Reykjanes Peninsula, SW Iceland: GPS measurements from 1993 to 1998. J. Geophys. Res. 106, 13803–13816.

Ívarsson, G., 1998. Fumarole gas geochemistry in estimating subsurface temperatures at Hengill in Southwestern Iceland. In: Arehart, G., Hulston, J.R. (Eds.), Water–Rock Interaction. Balkema, Rotterdam, pp. 459–462.

Massonnet, D., Feigl, K., 1998. Radar interferometry and its application to changes in the earth's surface. Rev. Geophys. 36, 441–500.

Massonnet, D., Sigmundsson, F., 1999. Remote sensing of volcanic deformation by radar interferometry from various satellites. In: Mouginis-Mark, P. (Ed.), Remote Sensing of Active Volcanoes. American Geophysical Union, Washington, DC, 271 pp.

Miller, A.D., Julian, B.R., Foulger, G.R., 1998. Three-dimensional seismic structure and moment tensors of non-double-couple earthquakes at the Hengill–Grensdalur volcanic complex, Iceland. Geophys. J. Int. 133, 309–325.

Rögnvaldsson, S., 1999 (in Icelandic).

Rögnvaldsson, S.Th., Árnadóttir, Þ., Águstsson, K., Skaftadóttir, Guðmundsson, G., Björnsson, G., Vogfjörð, K., Stefánsson, R., Böðvarsson, R., Slunga, R., Jakobsdóttir, S.S., Thorbjarnardóttir, B., Erlendsson, P., Bergsson, B., Ragnarsson, S., Halldósson, P., Thorkelsson, B., Asgeirsdóttir, M., 1998. Skjálftahrina í Ölfusi í nóvember. Icelandic Meteorological Office Report, VÍ-G98046-JA09 (with English summary).

Sæmundsson, K., 1967. Vulkanismus und Tektonik des Hengill-Gebietes in Südwest-Island. Acta Nat. Isl. 2, 105 pp.

Sæmundsson, K., 1978. Fissure swarms and central volcanoes of the neovolcanic zones of Iceland. In: Bowes, D.R., Leake, B.E. (Eds.), Crustal Evolution in NW-Britain and Adjacent Regions. Geol. J. Spec. Iss. 10, 415–432.

Sæmundsson, K., 1979. Outline of the geology of Iceland. Jökull 29, 7–28.

Sæmundsson, K., 1992. Geology of the Thingvallavatn area. Oikos 64, 40–68.

Sæmundsson, K., 1995. Hengill geological map (bedrock) 1:50 000. Orkustofnun, Hitaveita Reykjavikur, Landmælingar Íslands.

Sigmundsson, F., Einarsson, P., Bilham, R., Sturkell, E., 1995. Rift-transform kinematics in south Iceland: deformation from Global Positioning System measurements, 1986 to 1992. J. Geophys. Res. 100, 6235–6248.

Sigmundsson, F., Einarsson, P., Rögnvaldsson, S., Foulger, G.R., Hodgkinson, K.M., Thorbergsson, G., 1997. The 1994–1995 seismicity and deformation at the Hengill triple junction, Iceland: triggering of earthquakes by minor magma injection in a zone of horizontal shear stress. J. Geophys. Res. 102, 15151–15161.

Stefánsson, R., Böðvarsson, R., Slunga, R., Einarsson, P., Jakobsdóttir, S.S., Bungum, H., Gregersen, S., Havskov, J., Hjelme, J., Korhonen, H., 1993. Earthquake prediction research in the South Iceland seismic zone and the SIL project. Bull. Seismol. Soc. Am. 83, 696–716.

Thorbergsson, G., 1999. Nesjavallaveita GPS-mælinfar og mælingar yfir sprungur á Hengilssvæði 1999. Skýsla Orkustofnunar OS-99077.

Thorbergsson, G., Vigfusson, G.H., 1998. Nesjavallaveita Fallmælin og GPS-mælingar á Hengilssvæði. Skýsla Orkustofnunar OS-98060.